INORGANIC CHEMISTRY
FRONTIERS

RESEARCH ARTICLE

View Article Online
View Journal | View Issue

Cite this: *Inorg. Chem. Front.*, 2023, **10**, 2268

Structure and optical property evolution in PbM(PO_4)X (M = Zn, Sn; X = halogen): SHG effect and birefringence†

Xiao-Bao Li, Chun-Li Hu, Fang Kong * and Jiang-Gao Mao

Received 6th February 2023,
Accepted 7th March 2023

DOI: 10.1039/d3qi00230f

rsc.li/frontiers-inorganic

Four new phosphates, namely, PbZn(PO_4)F (**1**), PbSn(PO_4)Cl (**2**), PbSn(PO_4)Br (**3**) and PbSn(PO_4)I (**4**), were successfully synthesized by hydrothermal and solid-state reaction methods. PbZn(PO_4)F (**1**) was crystallized in a polar space group $Pna2_1$ and showed a significant SHG intensity of about 1.6 × KDP. PbSn(PO_4)Cl (**2**) and PbSn(PO_4)Br (**3**) were isostructural compounds, and they were crystallized in a monoclinic space group $P2_1/n$ while PbSn(PO_4)I (**4**) was crystallized in a triclinic space group $P\bar{1}$. PbZn(PO_4)F (**1**) features a new 3D framework while compounds **2**–**4** show a layered structure. Interestingly, the thermal stability and band gap of PbM(PO_4)X are decreased with an increase of the atomic number of the halogen atom, while the rule for birefringence is the opposite. Our work revealed the evolution effects of the halogen atoms on the structure and optical properties of PbM(PO_4)X compounds.

Introduction

As a functional material, nonlinear optical (NLO) materials are important components for expanding the wavelengths of lasers and enhancing the performance of laser light sources.[1–3] Over the decades, generations of researchers have built huge collections of NLO materials around their required characteristics, which include typical borates,[4–6] iodates,[7–9] chalcogenides[10–12] and phosphates.[13–16] Currently, metal phosphates are an important source for NLO material applications due to their structural advantages and good physicochemical properties, with familiar $KTiOPO_4$ (KTP) and KH_2PO_4 (KDP) being reported and successfully commercialized in the 1970s. In recent years, a series of novel metal phosphates were successfully explored as promising NLO materials, such as $LiPbPO_4$ (about 3 × KDP, 0.021@1064 nm),[17] Cs_2LiPO_4 (1.8 × KDP),[18] $LiHgPO_4$ (11 × KDP, 0.068@1064 nm),[19] $KMg(H_2O)PO_4$ (about 1.14 × KDP, 0.017@1064 nm),[20] $Rb_3PbBi(P_2O_7)_2$ (2.5 × KDP, 0.025@1064 nm),[21] $Bi_{32}Cd_3P_{10}O_{76}$ (about 4 × KDP),[22] β-$Cd(PO_3)_2$ (0.25 × KDP, 0.059@1064 nm),[23] $Na_3Sc_2(PO_4)_2F_3$ (0.26 × KDP, 0.0978@546.1 nm),[24] $CsMgPO_4{\cdot}6H_2O$ (1.36 × KDP, 0.0060@1064 nm),[25] $K_4Mg_4(P_2O_7)_3$ (1.3 × KDP, 0.0108@1064 nm),[26] and $K_2Sb(P_2O_7)F$ (4.0 × KDP, 0.157@546 nm).[27] However, the microscopic second-order multiplicity coefficients of the PO_4 group, the basic structural unit of phosphates, is much smaller than that of the BO_3 group, and the rigid PO_4 group also exhibits weak anisotropy, which greatly hampers the availability of phosphates in the field of NLO materials. After continuous exploration, researchers have concluded that the structure–property relationship of NLO materials,[28–30] that is, the optimization of the arrangement of building units or the introduction of other NLO-active building blocks into the target material, can be used to strengthen the SHG effect and birefringence of phosphates. These strategies include: (1) introducing metal ions with second-order Jahn–Teller distortion, such as KTP (about 12 × KDP, 0.090@1064 nm);[31] (2) breaking the symmetry of PO_4 groups, such as $NaNH_4PO_3F{\cdot}H_2O$ (1.1 × KDP, >0.053@589.3 nm);[32] and (3) introducing other anionic groups, such as $Cd_2(IO_3)(PO_4)$ (4 × KDP, 0.0108@1064 nm),[33] *etc*.

The Zn^{2+} cation, as a d^{10} transition metal (TM), has an 18*e* electron configuration with strong polarizability and significant deformability and will eliminate unwanted red shifts at the absorption edge.[34] In addition, Zn^{2+} can also exhibit various coordination configurations, such as ZnO_x (x = 4, 5, 6). Therefore, Zn^{2+} is proposed to be a premium NLO active building unit, which can increase the opportunities for the SHG property and birefringence magnitude if the asymmetric units are properly aligned.[35,36] Recently, some excellent Zn-based phosphates have been reported, such as $Rb_2Zn_3(P_2O_7)_2$ (1 ×

State Key Laboratory of Structural Chemistry, Fujian Institute of Research on the Structure of Matter, Chinese Academy of Sciences, Fuzhou 350002, P. R. China. E-mail: kongfang@fjirsm.ac.cn

†Electronic supplementary information (ESI) available: Experimental methods, crystal data, selected bond distances, PXRD patterns, IR and UV-vis-NIR diffuse reflectance spectra, thermal stability curves, band structures and SHG density map. CCDC 2237156–2237159. For ESI and crystallographic data in CIF or other electronic format see DOI: https://doi.org/10.1039/d3qi00230f

KDP),[37] $K_2ZnMoP_2O_{10}$ (about 6.8 × KDP, 0.0534@450.2 nm),[38] and $Ba_3(ZnB_5O_{10})PO_4$ (4 × KDP, 0.035@532 nm).[39] On the other hand, introducing metal cations with stereochemically active lone pairs (SCALP) has turned out to be a valid tactic for fabricating novel NLO and birefringence crystals.[40,41] In addition to the classical metal cations Pb^{2+} and Bi^{3+}, Sn^{2+} has also attracted a lot of attention in recent years. Emerging examples include $BaSn_2(PO_4)_2$ (0.07@1064 nm),[42] Sn_2PO_4X (X = F, Cl) (0.126@546 nm, 0.181@546 nm),[43] and Sn_2PO_4I (0.468@1064 nm),[44] demonstrating its great research potential.

Based on the above ideas and considering that different NLO active building units may have synergistic effects, we endeavored to combine SCALP Pb^{2+}, d^{10} TM Zn^{2+} or SCALP Sn^{2+} and halogen ions into the phosphate system to obtain new phosphate NLO materials. Four new lead halide phosphates, namely, $PbZn(PO_4)F$ (**1**), $PbSn(PO_4)Cl$ (**2**), $PbSn(PO_4)Br$ (**3**) and $PbSn(PO_4)I$ (**4**), based on the $PbM(PO_4)X$ formula, were synthesized successfully. $PbZn(PO_4)F$ (**1**) exhibited a significant SHG effect about 1.6 times as large as that of commercial KDP while $PbSn(PO_4)I$ (**4**) possessed a high birefringence intensity of 0.095 at 1064 nm. Interestingly, their structures and optical properties evolved simultaneously with the alteration of halogen elements. In this work, we present their syntheses, crystallographic structures, optical properties and related theoretical calculations.

Experimental section

Materials

All materials were of analytical purity grade, were commercially available, and used as received. Lead oxide (PbO), tin(II) oxide (SnO), ammonium dihydrogen phosphate ($NH_4H_2PO_4$), tin(II) chloride ($SnCl_2$), tin(II) bromide ($SnBr_2$), phosphorus pentoxide (P_2O_5), zinc fluoride (ZnF_2), hydrofluoric acid (HF, 35%), hydrochloric acid (HCl, 37%), hydroiodic acid (HI, ≥47%) and phosphoric acid (H_3PO_4, 85%) were obtained from Aladdin.

Synthesis

The four compounds were synthesized utilizing two different approaches. Compounds $PbZn(PO_4)F$ (**1**), $PbSn(PO_4)Cl$ (**2**) and $PbSn(PO_4)I$ (**4**) were synthesized by a mild hydrothermal method. The starting reagents are PbO (1 mmol), ZnF_2 (1.1 mmol), $NH_4H_2PO_4$ (1 mmol), HF (0.1 mL), H_3PO_4 (0.8 mL) and H_2O (3 mL) for **1**; PbO (1 mmol), $SnCl_2$ (1 mmol), $NH_4H_2PO_4$ (1 mmol), (0.1 mL), H_3PO_4 (0.8 mL) and H_2O (3 mL) for **2**; and PbO (1 mmol), SnO (1 mmol), HI (0.15 mL), H_3PO_4 (0.6 mL) and H_2O (3.0 mL) for **4**. The above mixtures were transferred to an oven and heated at 230 °C, 190 °C and 210 °C for 72 h, respectively. Colourless rod-like crystals of $PbZn(PO_4)F$ (**1**) were obtained in a yield of 63% (based on Pb, the same as below). Tiny sheet-like crystals of $PbSn(PO_4)Cl$ (**2**) were mixed with some unknown impurities, which were difficult to separate from the product. We tried to obtain its pure phase by changing the experimental conditions, but failed. Yellow sheet-like crystals of $PbSn(PO_4)I$ (**4**) were obtained in a yield of 45%. Compound $PbSn(PO_4)Br$ (**3**) was synthesized by a high-temperature solid-state reaction. The raw materials of PbO, $SnBr_2$, and P_2O_5 were well ground in a molar ratio of 1 : 1 : 1 in a glovebox and placed in a quartz tube, which was sealed at 10^{-3} Pa. The sample was heated at 650 °C for 48 h, and cooled to 480 °C at 2 °C h^{-1} before the muffle furnace was turned off. Impurities were washed away with distilled water. Clean crystals of **3** were obtained in a yield of 40%.

Single-crystal structure determination

Appropriately sized crystals of the four compounds were selected for structure determination. Crystal data were collected by operating a SuperNona CCD diffractometer with graphite monochromatic Mo Kα radiation (λ = 0.71073 Å). The collected data were subjected to cell refinement and data reduction using *CrysAlisPro* software, and the absorption correction processing was performed by the multi-scan method. Direct analysis of the structures was conducted using the SHELXTL-97 program with a full matrix least-squares fitting on F^2.[45] The structures were further checked using PLATON and no higher symmetries were observed.[46] Relevant crystallographic data are outlined in Table S1.† The selected bond lengths are outlined in Table S2.†

Powder X-ray diffraction

Powder X-ray diffraction (PXRD) data were recorded on a Miniflex 600 powder X-ray diffractometer at room temperature (RT) with Cu Kα radiation (λ = 1.540598 Å, 2θ = 10°–70°, increment = 0.02°). The PXRD plots of the compounds are presented in Fig. S1.†

UV-vis-NIR diffuse reflectance and infrared spectra

The UV-vis-NIR diffuse reflectance spectra (200–2000 nm) were recorded on a PerkinElmer Lamda-950 spectrophotometer; a powder $BaSO_4$ plate served as the 100% reflectivity reference. The experimental band gaps were made available by the calculation of the absorption value from the reflection spectra following the Kubelka–Munk function.[47] The infrared spectra (IR, 4000–400 cm^{-1}) were recorded on a Magna 750 FT-IR spectrometer, with air serving as the background, to verify the P–O bonds in these compounds.

Thermal analysis

Thermal stability measurements were carried out under a constant N_2 flow on a NETZSCH STA 449C simultaneous analyzer (heating rate: 15 °C min^{-1}; temperature range: 20–1000 °C).

Second-harmonic generation

Powder second-harmonic generation (SHG) measurements were performed at RT using a Q-switched Nd:YAG laser at a wavelength of 1064 nm, following the Kurtz–Perry method. The output light intensity emitted from the samples was measured using a photomultiplier tube, and the same size of crystalline KDP (70–100 mesh) was used as the reference.[48]

Results and discussion

Structure of $PbZn(PO_4)F$

$PbM(PO_4)X$ features three different structures and we obtained the pure phases of compounds **1**, **3** and **4** successfully (Fig. S1†). $PbZn(PO_4)F$ is crystallized in the polar space group $Pna2_1$ (No. 33) and exhibited a 3D framework that was constructed from PO_4 groups, ZnO_4F triangular bipyramids and PbO_2F_2 units. Its asymmetric unit contained one Pb, one Zn, one P, one halogen and four O atoms. The P(1) atom coordinated with four O atoms to shape the tetrahedral configuration and the P–O bond lengths ranged from 1.515(11) to 1.551(8) Å. The Zn(1) atom was coordinated with one F and four O atoms, giving rise to a highly distorted triangular bipyramid, in which the bond angle of F(1)–Zn(1)–O(1) is equal to 161.3(3)° (Fig. 1a). The Pb(1) atom was coupled to two O atoms and two F atoms with Pb–O/F bond lengths in the range of 2.359(7)–2.514(10) Å. Due to the repulsion of the lone-pair electrons on Pb, the O and F atoms were gathered on one side of the Pb atom, resulting in a "seesaw" model of the PbO_2F_2 unit. The bond value calculations showed that the bond valences of Pb(1), Zn(1), P(1) and F(1) were 1.84, 2.07, 4.85 and 0.96, respectively, suggesting their oxidation states of +2, +2, +5 and −1, respectively.[49,50]

The distorted ZnO_4F triangular bipyramids and the PO_4 tetrahedra were interconnected alternately into a 3D $[Zn(PO_4)F]^{2-}$ anionic framework with four- and eight-member polyhedral ring (MPR) tunnels along the *c*-axis (Fig. 1b and c). The PbO_2F_2 units form a 1D $[PbO_2F_2]^{4-}$ chain along the *c*-axis (Fig. S2†), located at large eight-MPR tunnels. Viewed from the *a*-axis, there were six-member polyhedral ring tunnels, containing the Pb atoms, in the $[Zn(PO_4)F]^{2-}$ anionic framework (Fig. 1d).

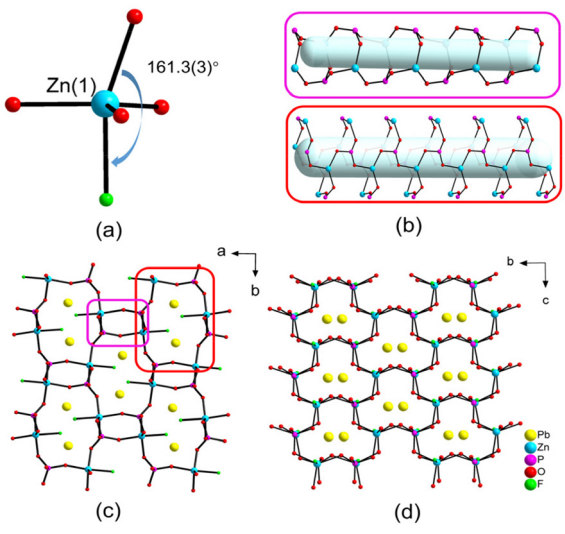

Fig. 1 The ZnO_4F triangular bipyramid (a), the 1D four-MPR channel (purple rectangle) and the eight-MPR channel (red rectangle) (b), the 3D structure of $PbZn(PO_4)F$ along the *c*-axis (c) and the *a*-axis (d) (the Pb–O and Pb–F bonds have been neglected for clarity).

Structures of $PbSn(PO_4)Br$ and $PbSn(PO_4)I$

$PbSn(PO_4)Cl$ (**2**) and $PbSn(PO_4)Br$ (**3**) were isostructural and crystallized in the monoclinic space group $P2_1/n$ (No. 14). However, $PbSn(PO_4)I$ (**4**) crystallized in the triclinic space group $P\bar{1}$ (No. 2). The asymmetric units of compounds **2**–**4** were similar to $PbZn(PO_4)F$ (**1**), including one Pb, one Sn, one P, one halogen and four O atoms. All of the P(1) atoms coupled with four O atoms to shape a pyramidal configuration with the P–O bond distances ranging from 1.525(10) to 1.56(2) Å. The Sn(1) atom was coordinated with three O atoms to form a SnO_3 triangular pyramid, in which the range of Sn–O bond distances was 2.104(19)–2.232(9) Å. The Pb atom was connected to four O atoms and one halogen atom in a PbO_4X polyhedron. The Pb–O bond distances ranged from 2.426(9) to 2.74(2) Å, and the corresponding Pb–X bond distance was 2.830(4), 2.9770(15) and 3.135(2) Å for the Cl, Br and I compounds, respectively. The bond value calculation results showed that the bond valences of Pb, Sn, P and Cl/Br/I were 2.02/2.08/1.98, 1.90/1.81/1.90, 4.81/4.82/4.73, and 0.75/0.82/0.78, respectively, which suggests that the valences of Pb, Sn, P and halogen elements in the structures of **2**–**4** were +2, +2, +5 and −1, respectively.

Although the space groups of compounds **3** and **4** were different, their structures were very similar. In their structures, the PO_4 tetrahedra and the SnO_3 triangular pyramids were interconnected alternately into a $[Sn(PO_4)_2]^{4-}$ chain with 1D four-MPR tunnels (Fig. 2a). Two PbO_4X polyhedra were edge-shared into a $Pb_2O_6X_2$ dimer by oxygen atoms (Fig. 2b). The $[Sn(PO_4)_2]^{4-}$ chains were bridged by the $Pb_2O_6X_2$ dimers into a 2D layered structure (Fig. 2c and d). In the structure of $PbSn(PO_4)I$ (**4**), the neighboring layers were identical while there was a two-fold axis between the neighboring layers of $PbSn(PO_4)Br$ (**3**). That is, the difference between compounds **3** and **4** is caused by different arrangements of the $PbSn(PO_4)X$ layers.

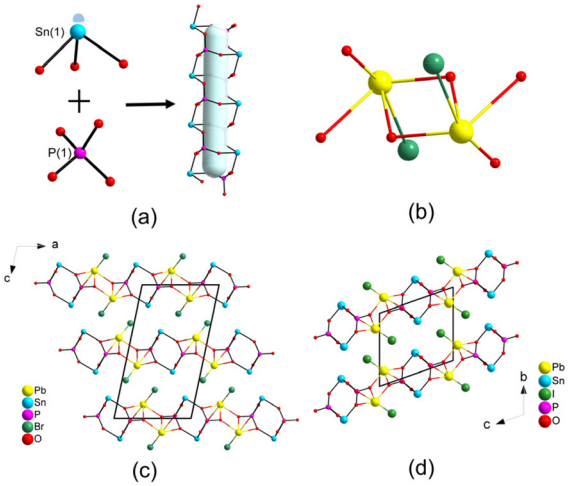

Fig. 2 The SnO_3 group, PO_4 group and $[Sn(PO_4)_2]^{4-}$ chain (a), $Pb_2O_6X_2$ dimer (b), the framework of $PbSn(PO_4)Br$ (c) and $PbSn(PO_4)I$ (d).

Based on the above analysis, we can find that the structural symmetry of $PbM(PO_4)X$ decreased from an orthogonal, monoclinic, to a triclinic system when the halogen atom was changed from fluorine to iodine. The F atoms in $PbZn(PO_4)F$ coordinated with Pb and Zn simultaneously while the halogen in $PbSn(PO_4)X$ can only link with Pb atoms. Due to the high coordination number of Zn, compared with that of Sn, a 3D open framework was formed by the zinc and phosphate polyhedra in $PbZn(PO_4)F$ while the SnO_3 and PO_4 groups could only form 1D $[Sn(PO_4)_2]^{4-}$ chains in the structure of $PbSn(PO_4)X$. The lead oxyhalide groups in $PbZn(PO_4)F$ haven't participated in the expansion of the structural dimension while the PbO_4X polyhedra in $PbSn(PO_4)X$ bridged the $[Sn(PO_4)_2]^{4-}$ chains into a 2D layered structure. The interlayer distances are increased from 7.3 and 7.5 to 8.7 Å when the halogen changed from Cl and Br to I. The sharp increase of the interlayer distance of $PbSn(PO_4)I$ corresponds to the obvious enhancement of the atomic radius of I from Br.

IR and UV-vis-NIR diffuse reflectance spectra

The IR spectra of compounds **1**, **3** and **4** are represented in Fig. S3.† The P–O stretching vibrations fall in the regions of 1086–921, 1074–937 and 1080–964 cm^{-1}, while the bending vibrations fall essentially in the region of 600–400 cm^{-1}.[51,52] The UV-vis-NIR diffuse reflectance spectra of compounds **1**, **3** and **4** revealed that they exhibited wide transparency ranges from 500 to 2000 nm (Fig. S4†). The cut-off edges of compounds **1**, **3** and **4** were 229, 310 and 319 nm, and the corresponding optical band gaps were 4.38, 3.30, and 2.60 eV, respectively. The band gap of $PbM(PO_4)X$ decreased with the increase of the atomic number of the halogen element, while the absorption edge of compound **1** was significantly blue shifted due to the incorporation of the d^{10} TM and the fluorine element.

Thermal stability tests

Thermal stability tests for these three compounds were conducted in the temperatures range of 30–1000 °C. As shown in Fig. S5,† the three compounds started to break down at 660 °C, 565 °C and 554 °C respectively, and their thermal stability decreased with the increase of the atomic weight of halogen atoms. The compounds showed one step of weight loss. The total weight loss of $PbZn(PO_4)F$ (**1**) was 3.8%, corresponding to the partial release of the fluorine element. The total weight losses of compound **3** and **4** were 21.0% and 35.2%, respectively, which can be ascribed to the decomposition of the stannous halides.

SHG characterization

$PbZn(PO_4)F$ (**1**) crystallized in the non-centrosymmetric space group. The sieved (70–100 mesh) $PbZn(PO_4)F$ (**1**) crystal samples were tested under the illumination of a Q-switched Nd:YAG 1064 nm laser to investigate its SHG behaviour. Likewise, the same size of KDP crystal served as a reference. The results revealed that $PbZn(PO_4)F$ (**1**) exhibited a strong frequency doubling intensity, approximately 1.6 times that of the commercial KDP (Fig. 3), exceeding the SHG intensity of many other phosphates, uch as $KMg(H_2O)PO_4$ (about 1.14 × KDP),[20] $Ba_3[Al(PO_4)_3]$ (about 0.5 × KDP),[14] $Rb_2Zn_3(P_2O_7)_2$ (1 × KDP),[37] $K_2SrP_4O_{12}$(0.5 × KDP),[15] $CsMgPO_4{\cdot}6H_2O$ (1.36 × KDP),[25] *etc*. To further reveal the relationship between the SHG effect and the functional units, it is necessary to illustrate the SHG density map of the maximum tensors d_{33} in the valence band (VB) and the conduction band (CB) of $PbZn(PO_4)F$ (Fig. S6†). The SHG effect contributions to the VB were largely accounted for by the Zn-3d, O-2p and F-2p non-bonded electronic states; the SHG contribution in the CB was largely accounted for by the Pb-6p non-occupied orbitals. From the overall SHG density, the SHG contributions of each unit (PO_4, PbO_2F_2 and ZnO_4F groups) in $PbZn(PO_4)F$ (**1**) were estimated to be 40.21%, 37.66% and 22.13%, respectively, indicating the synergistic effect of the anionic groups.

Optical property calculation

The optical properties of these compounds, involving SHG and birefringence, were simulated with the help of the DFT method. The simulated band gap structures revealed that compounds **1**–**3** showed different *K* points in the lowest CB and highest VB in the first Brillouin zone, indicating that they were all indirect band gap compounds with band gaps of 4.44, 2.57 and 2.78 eV, respectively. The lowest VB and the highest CB of compound **4** both fell at the *Z* point, that is, a direct band gap compound with a band gap of 2.58 eV (Fig. S7†). Details of the state energies are categorized in Table S3.† Due to the natural limitation of the GGA-PBE functional in the DFT method, the experimental band gap was often a bit higher than the calculated one. Therefore, the scissors of 0, 0.54 and 0.02 eV were adopted for compounds **1**, **3** and **4**, respectively, in this work.

The partial density of states (PDOS) for $PbZn(PO_4)F$ (**1**) is displayed in Fig. 4a. The low-energy interval −22 to −9 eV in the VB was largely controlled by the Pb-5d, O-2s and F-2s states. The energy interval of −9 to 0 eV was mostly filled by Zn-3d, O-2p and F-2p states. The O-2p nonbonding orbitals governed the top of the VB. The bottom of the CB originated from Pb-6p states. Thus, the band gap of $PbZn(PO_4)F$ (**1**) is

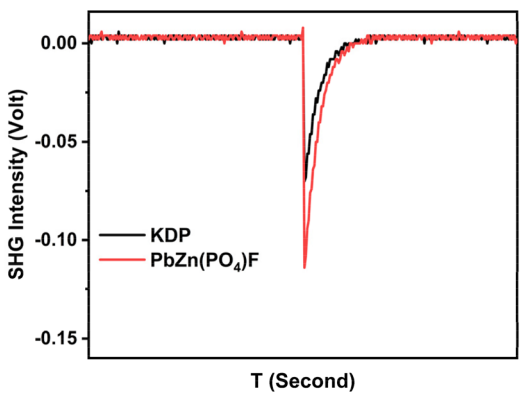

Fig. 3 SHG intensity of sieved $PbZn(PO_4)F$ (70–100 mesh) with KDP as the background.

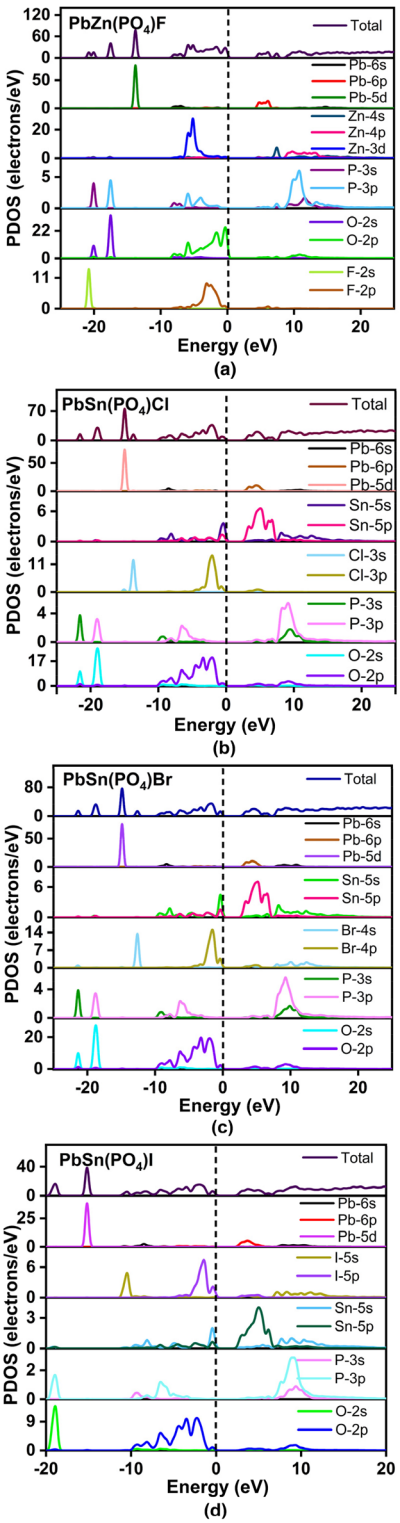

Fig. 4 The PDOS for $PbZn(PO_4)F$ (a), $PbSn(PO_4)Cl$ (b), $PbSn(PO_4)Br$ (c) and $PbSn(PO_4)I$ (d).

controlled by O and Pb atoms. The PDOS plots for compounds **2–4** were comparable (Fig. 4b–d). In the case of $PbSn(PO_4)Br$ (**3**), for example, the lower energy interval of −22 to −10 eV in the VB was strongly influenced by the Pb-5d, O-2s and Br-4s states. The energy level interval of −9 to 0 eV was mostly filled by O-2p, Br-4p and Sn-5s states. The bottom of the CB was mainly formed by Pb-6p and Sn-5p states. The O-2p and Br-4p

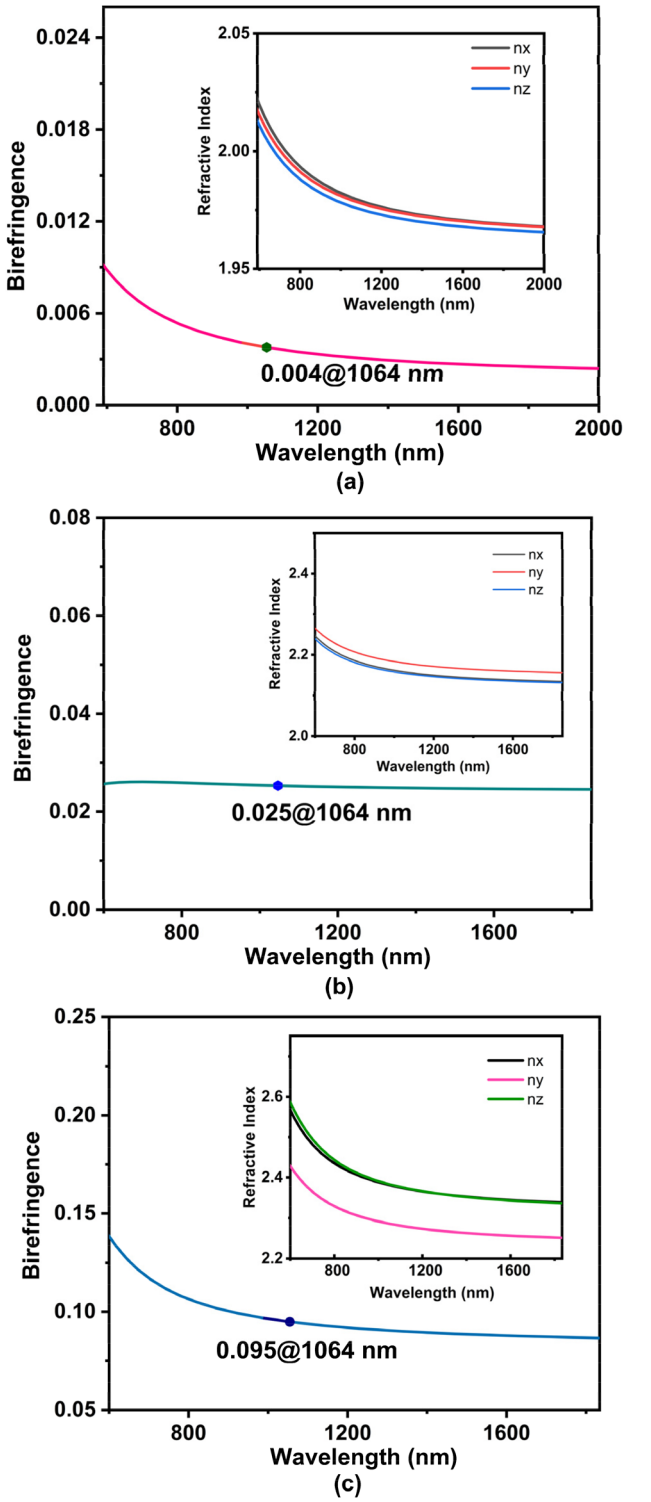

Fig. 5 The birefringence of $PbZn(PO_4)F$ (a), $PbSn(PO_4)Br$ (b) and $PbSn(PO_4)I$ (c).

nonbonding orbitals governed the top of the VB. Thus, the band gap of $PbSn(PO_4)X$ is determined by X, O and Pb atoms.

As mentioned previously, compounds **1**, **3** and **4** are crystallized in the orthorhombic, monoclinic and triclinic crystal systems, respectively, and they belong to biaxial crystals, that is, the three major permittivity coefficients of the three compounds were not equal, $\varepsilon_1 \neq \varepsilon_2 \neq \varepsilon_3$, and thus the refractive indices were also not equal, $n_1 \neq n_2 \neq n_3$. Here, the birefringence can be obtained by the equation $\Delta n = n_{max} - n_{min}$ (Fig. 5). The anisotropy of $PbZn(PO_4)F$ (**1**) was very weak, with a birefringence of 0.004 at 1064 nm, making it difficult to satisfy the general angular phase matching conditions. However, the small birefringence (less than 0.01) makes $PbZn(PO_4)F$ (**1**) a potential candidate for zero-order waveplates.[53] For compounds **3** and **4**, the n_x and n_z curves follow the same direction and are even partially overlapped, but they are far from the n_y curves. The birefringence of compound **3** was calculated to be 0.025 at 1064 nm and that of compound **4** was 0.095 at 1064 nm. Thus, the birefringence of $PbM(PO_4)X$ increased with increasing atomic number of the halogen element. The birefringence values of some phosphates are presented in Table S4.† Simple phosphates usually have small birefringence, and the introduction of functional units may solve this problem.

Conclusions

In summary, four new phosphates with a $PbM(PO_4)X$ formula, namely, $PbZn(PO_4)F$ (**1**), $PbSn(PO_4)Cl$ (**2**), $PbSn(PO_4)Br$ (**3**) and $PbSn(PO_4)I$ (**4**), were synthesized and characterized successfully. $PbZn(PO_4)F$ (**1**) was crystallized in a polar space group $Pna2_1$ and it showed a moderate SHG intensity of about 1.6 × KDP. The 3D structure consisted of a 3D $[Zn(PO_4)F]^{2-}$ anionic framework with lead atoms located in the eight-MPR tunnels. Compounds **2**–**4** crystallized in the CS space group and their layered structures were similar, composed of $[Sn(PO_4)_2]^{4-}$ chains bridged by $Pb_2O_6X_2$ dimers, although the crystal symmetry of $PbSn(PO_4)I$ (**4**) was lower than those of the isostructural compounds **2** and **3**. In addition to the crystal symmetry, the thermal stability and the band gap of the compounds also decreased with an increase of the atomic number of the halogen. The NCS $PbZn(PO_4)F$ (**1**) was the most stable of these four compounds (660 °C) and featured the largest band gap (4.38 eV). However, the birefringence is increased with an increase of the atomic weight of halogen. Of the title compounds, the highest birefringence of 0.095 at 1064 nm was observed for $PbSn(PO_4)I$ (**4**). This work proved that the halogen elements can effectively regulate the structure and optical properties of oxyhalide compounds.

Conflicts of interest

There are no conflicts to declare.

Acknowledgements

This work was supported by the National Natural Science Foundation of China (Grants No.: 91963105, 22031009 and 21921001).

References

1 P. F. Bordui and M. Fejer, Inorganic Crystals for Nonlinear Optical Frequency Conversion, *Annu. Rev. Mater. Sci.*, 1993, **23**, 321–379.
2 A. R. S. Suresh, D. Jayaraman and a. P. Mani, Review on theoretical aspect of nonlinear optics, *Rev. Adv. Mater. Sci.*, 2012, **30**, 175–183.
3 S.-P. Guo, Y. Chi and G.-C. Guo, Recent achievements on middle and far-infrared second-order nonlinear optical materials, *Coord. Chem. Rev.*, 2017, **335**, 44–57.
4 Y.-N. Zhang, Q.-F. Li, B.-B. Chen, Y.-Z. Lan, J.-W. Cheng and G.-Y. Yang, $Na_3B_6O_{10}(HCOO)$: an ultraviolet nonlinear optical sodium borate-formate, *Inorg. Chem. Front.*, 2022, **9**, 5032–5038.
5 Y. Li, X. Chen and K. M. Ok, $KF{\cdot}B(OH)_3$: a KBBF-type material with large birefringence and remarkable deep-ultraviolet transparency, *Chem. Commun.*, 2022, **58**, 8770–8773.
6 J. Jiao, M. Zhang and S. Pan, Aluminoborates as Nonlinear Optical Materials, *Angew. Chem., Int. Ed.*, 2022, e202217037.
7 C. Wu, L. Lin, X. Jiang, Z. Lin, Z. Huang, M. G. Humphrey, P. S. Halasyamani and C. Zhang, $K_5(W_3O_9F_4)(IO_3)$: An Efficient Mid-Infrared Nonlinear Optical Compound with High Laser Damage Threshold, *Chem. Mater.*, 2019, **31**, 10100–10108.
8 J. Chen, C. L. Hu, F. F. Mao, B. P. Yang, X. H. Zhang and J. G. Mao, REI_5O_{14} (RE = Y and Gd): Promising SHG Materials Featuring the Semicircle-Shaped $I_5O_{14}^{3-}$ Polyiodate Anion, *Angew. Chem., Int. Ed.*, 2019, **58**, 11666–11669.
9 C. Wu, G. Wei, X. Jiang, Q. Xu, Z. Lin, Z. Huang, M. G. Humphrey and C. Zhang, Additive-Triggered Polar Polymorph Formation: beta-$Sc(IO_3)_3$, a Promising Next-Generation Mid-Infrared Nonlinear Optical Material, *Angew. Chem., Int. Ed.*, 2022, **61**, e202208514.
10 J. Chen, Y. Zhang, H. Wu, Z. Hu, J. Wang, Y. Wu and H. Yu, $AeMg_6Ga_6S_{16}$ (Ae = Ca, Sr, Ba): The First Double Alkaline-Earth Metal Chalcogenides with Excellent Performances, *Adv. Opt. Mater.*, 2022, **11**, 2202147–2202155.
11 S.-F. Li, X.-M. Jiang, B.-W. Liu, D. Yan, C.-S. Lin, H.-Y. Zeng and G.-C. Guo, Superpolyhedron-Built Second Harmonic Generation Materials Exhibit Large Mid-Infrared Conversion Efficiencies and High Laser-Induced Damage Thresholds, *Chem. Mater.*, 2017, **29**, 1796–1804.
12 X. Luo, Z. Li, F. Liang, Y. Guo, Y. Wu, Z. Lin and J. Yao, Synthesis, Structure, and Characterization of Two Mixed-Cation Quaternary Chalcogenides K_2BaSnQ_4 (Q = S, Se), *Inorg. Chem.*, 2019, **58**, 7118–7125.

13 W. Dong, Y. Sun, Q. Yao, Q. Wang, H. Wen, J. Li, X. Xu and J. Wang, $Te_3O_3(PO_4)_2$: a phosphate crystal with large birefringence activated by the highly distorted [TeO_5] group and antiparallel [PO_4] pseudo-layer, *J. Mater. Chem. C*, 2020, **8**, 9585–9592.

14 V. V. Atuchin, V. G. Kesler, G. Meng and Z. S. Lin, The electronic structure of $RbTiOPO_4$ and the effects of the A-site cation substitution in $KTiOPO_4$-family crystals, *J. Phys.: Condens. Matter*, 2012, **24**, 405503.

15 Z. Bai, L. Liu, L. Zhang, Y. Huang, F. Yuan and Z. Lin, $K_2SrP_4O_{12}$: a deep-UV transparent cyclophosphate as a nonlinear optical crystal, *Chem. Commun.*, 2019, **55**, 8454–8457.

16 J. L. Xie, Y. H. Zhou, L. H. Li, J. H. Zhang and J. L. Song, A new method for the preparation of a $[Sn_2(H_2PO_2)_3]Br$ SHG-active polar crystal via surfactant-induced strategy, *Dalton Trans.*, 2017, **46**, 9339–9343.

17 G. Han, Q. Liu, Y. Wang, X. Su, Z. Yang and S. Pan, Experimental and theoretical studies on the linear and nonlinear optical properties of lead phosphate crystals $LiPbPO_4$, *Phys. Chem. Chem. Phys.*, 2016, **18**, 19123–19129.

18 Y. Shen, Y. Yang, S. Zhao, B. Zhao, Z. Lin, C. Ji, L. Li, P. Fu, M. Hong and J. Luo, Deep-Ultraviolet Transparent Cs_2LiPO_4 Exhibits an Unprecedented Second Harmonic Generation, *Chem. Mater.*, 2016, **28**, 7110–7116.

19 B. L. Wu, C. L. Hu, F. F. Mao, R. L. Tang and J. G. Mao, Highly Polarizable Hg^{2+} Induced a Strong Second Harmonic Generation Signal and Large Birefringence in $LiHgPO_4$, *J. Am. Chem. Soc.*, 2019, **141**, 10188–10192.

20 Z. Bai, C.-L. Hu, L. Liu, L. Zhang, Y. Huang, F. Yuan and Z. Lin, $KMg(H_2O)PO_4$: A Deep-Ultraviolet Transparent Nonlinear Optical Material Derived from $KTiOPO_4$, *Chem. Mater.*, 2019, **31**, 9540–9545.

21 L. Qi, Z. Chen, X. Shi, X. Zhang, Q. Jing, N. Li, Z. Jiang, B. Zhang and M.-H. Lee, $A_3BBi(P_2O_7)_2$ (A = Rb, Cs; B = Pb, Ba): Isovalent Cation Substitution to Sustain Large Second-Harmonic Generation Responses, *Chem. Mater.*, 2020, **32**, 8713–8723.

22 J. Wang, B. Xiong, H. Wu, H. Yu, Z. Hu, J. Wang and Y. Wu, $Bi_{32}Cd_3P_{10}O_{76}$: a new congruently melting nonlinear optical crystal with a large SHG response and a wide transparent region, *Inorg. Chem. Front.*, 2021, **8**, 344–351.

23 J. Lv, Y. Qian, Q. Jing, X. Wang, M.-H. Lee and Z. Chen, Two Metal Phosphate Nonlinear Optical Materials Simultaneously Exhibiting Ultraviolet Transparence and a Large Birefringence, *Chem. Mater.*, 2022, **34**, 5919–5927.

24 F. Xu, G. Peng, C. Lin, D. Zhao, B. Li, G. Zhang, S. Yang and N. Ye, $Na_3Sc_2(PO_4)_2F_3$: rational design and synthesis of an alkali rare-earth phosphate fluoride as an ultraviolet nonlinear optical crystal with an enlarged birefringence, *J. Mater. Chem. C*, 2020, **8**, 4965–4972.

25 Y. Zhou, L. Cao, C. Lin, M. Luo, T. Yan, N. Ye and W. Cheng, $AMgPO_4{\cdot}6H_2O$ (A = Rb, Cs): strong SHG responses originated from orderly PO_4 groups, *J. Mater. Chem. C*, 2016, **4**, 9219–9226.

26 H. Yu, J. Young, H. Wu, W. Zhang, J. M. Rondinelli and P. S. Halasyamani, $M_4Mg_4(P_2O_7)_3$ (M = K, Rb): Structural Engineering of Pyrophosphates for Nonlinear Optical Applications, *Chem. Mater.*, 2017, **29**, 1845–1855.

27 Y. Deng, L. Huang, X. Dong, L. Wang, K. M. Ok, H. Zeng, Z. Lin and G. Zou, $K_2Sb(P_2O_7)F$: Cairo Pentagonal Layer with Bifunctional Genes Reveal Optical Performance, *Angew. Chem., Int. Ed.*, 2020, **59**, 21151–21156.

28 Y. Li, J. Luo and S. Zhao, Local Polarity-Induced Assembly of Second-Order Nonlinear Optical Materials, *Acc. Chem. Res.*, 2022, **55**, 3460–3469.

29 C. Wu, G. Yang, M. G. Humphrey and C. Zhang, Recent advances in ultraviolet and deep-ultraviolet second-order nonlinear optical crystals, *Coord. Chem. Rev.*, 2018, **375**, 459–488.

30 H. Yu, W. Zhang, J. Young, J. M. Rondinelli and P. S. Halasyamani, Bidenticity-Enhanced Second Harmonic Generation from Pb Chelation in $Pb_3Mg_3TeP_2O_{14}$, *J. Am. Chem. Soc.*, 2016, **138**, 88–91.

31 F. Yang, L. Wang, L. Huang and G. Zou, The study of structure evolvement of $KTiOPO_4$ family and their nonlinear optical properties, *Coord. Chem. Rev.*, 2020, **423**, 213491.

32 J. Lu, J. N. Yue, L. Xiong, W. K. Zhang, L. Chen and L. M. Wu, Uniform Alignment of Non-π-Conjugated Species Enhances Deep Ultraviolet Optical Nonlinearity, *J. Am. Chem. Soc.*, 2019, **141**, 8093–8097.

33 Q. Q. Chen, C. L. Hu, L. J. Yao, J. Chen, M. Y. Cao, B. X. Li and J. G. Mao, $Cd_2(IO_3)(PO_4)$ and $Cd_{1.62}Mg_{0.38}(IO_3)(PO_4)$: metal iodate-phosphates with large SHG responses and wide band gaps, *Chem. Commun.*, 2022, **58**, 7694–7697.

34 T. Yu, L. Xiong, X. Liu, Y.-C. Yang, Z. Lin, L.-M. Wu and L. Chen, $AZn(PO_3)_3$ (A = K, Rb): Deep-Ultraviolet Nonlinear Optical Phosphates Derived from Synergy of a Unique [ZnO_6] Octahedron and a $[PO_3]_\infty$ Chain, *Cryst. Growth Des.*, 2021, **21**, 2445–2452.

35 L. Zhou, S. Pan, X. Dong, H. Yu, H. Wu, F. Zhang and Z. Zhou, $Na_2Cd_7B_8O_{20}$: a new noncentrosymmetric compound with special [B_3O_7] units, *CrystEngComm*, 2013, **15**, 3412–3416.

36 X. Pan, M. Wen, G. He, H. Li and D. Jia, Syntheses, structures and properties of metal phosphates $Pb_2Mg(PO_4)_2$, $Pb_4Zn_8(PO_4)_8$ and alpha-$BaZn_2(PO_4)_2$, *Dalton Trans.*, 2017, **46**, 16034–16040.

37 Z. Song, H. Yu, H. Wu, Z. Hu, J. Wang and Y. Wu, Syntheses, structures and characterization of non-centrosymmetric $Rb_2Zn_3(P_2O_7)_2$ and centrosymmetric $Cs_2M_3(P_2O_7)_2$ (M = Zn and Mg), *Inorg. Chem. Front.*, 2020, **7**, 3482–3490.

38 H. Liu, H. Wu, H. Yu, Z. Hu, J. Wang and Y. Wu, $K_2ZnMoP_2O_{10}$: a novel nonlinear optical molybdophosphate with a strong second harmonic generation response and moderate birefringence, *J. Mater. Chem. C*, 2021, **9**, 15321–15328.

39 H. Yu, W. Zhang, J. Young, J. M. Rondinelli and P. S. Halasyamani, Design and Synthesis of the Beryllium-Free Deep-Ultraviolet Nonlinear Optical Material $Ba_3Zn(B_5O_{10})PO_4$, *Adv. Mater.*, 2015, **27**, 7380–7385.

40 Q. Wei, C. He, K. Wang, X. F. Duan, X. T. An, J. H. Li and G. M. Wang, $Sb_6O_7(SO_4)_2$: A Promising Ultraviolet Nonlinear Optical Material with an Enhanced Second-Harmonic-Generation Response Activated by Sb^{III} Lone-Pair Stereoactivity, *Chem. – Eur. J.*, 2021, **27**, 5880–5884.

41 Y. J. Jia, X. Zhang, Y. G. Chen, X. Jiang, J. N. Song, Z. Lin and X. M. Zhang, $PbBi(SeO_3)_2F$ and $Pb_2Bi(SeO_3)_2Cl_3$: Coexistence of Three Kinds of Stereochemically Active Lone-Pair Cations Exhibiting Excellent Nonlinear Optical Properties, *Inorg. Chem.*, 2022, **61**, 15368–15376.

42 Y. Yang, Y. Qiu, P. Gong, L. Kang, G. Song, X. Liu, J. Sun and Z. Lin, Lone-Pair Enhanced Birefringence in an Alkaline-Earth Metal Tin(II) Phosphate $BaSn_2(PO_4)_2$, *Chem. – Eur. J.*, 2019, **25**, 5648–5651.

43 T. Zheng, Q. Wang, J. Ren, L. Cao, L. Huang, D. Gao, J. Bi and G. Zou, Halogen regulation triggers structural transformation from centrosymmetric to noncentrosymmetric switches in tin phosphate halides Sn_2PO_4X (X = F, Cl), *Inorg. Chem. Front.*, 2022, **9**, 4705–4713.

44 J. Guo, A. Tudi, S. Han, Z. Yang and S. Pan, Sn_2PO_4I: An Excellent Birefringent Material with Giant Optical Anisotropy in Non π-Conjugated Phosphate, *Angew. Chem., Int. Ed.*, 2021, **60**, 24901–24904.

45 G. M. Sheldrick, Crystal structure refinement with SHELXL, *Acta Crystallogr., Sect. C: Struct. Chem.*, 2015, **71**, 3–8.

46 A. L. Spek, Single-crystal structure validation with the program PLATON, *J. Appl. Crystallogr.*, 2003, **36**, 7–13.

47 F. M. P. Kubelka, An Article on Optics of Paint Layers, *Z. Tech. Phys.*, 1931, **12**, 886–892.

48 S. K. Kurtz and T. T. Perry, A Powder Technique for the Evaluation of Nonlinear Optical Materials, *J. Appl. Phys.*, 1968, **39**, 3798–3813.

49 M. O. K. N. Brese, Bond-valence parameters for solids, *Acta Crystallogr., Sect. B: Struct. Sci.*, 1991, **47**, 192–197.

50 D. A. I. Brown, Bond–valence parameters obtained from a systematic analysis of the Inorganic Crystal Structure Database, *Acta Crystallogr., Sect. B: Struct. Sci.*, 1985, **41**, 244–247.

51 D. Balaji, T. R. Mandlimath, J. Chen, Y. Matsushita and S. P. Kumar, Langbeinite Phosphates $KPbM_2(PO_4)_3$ (M = Cr, Fe): Synthesis, Structure, Thermal Expansion, and Magnetic Properties Investigation, *Inorg. Chem.*, 2020, **59**, 13245–13253.

52 M. Wen, H. Wu and X. Wu, Influence of Cation on the Anion Frameworks and Properties of Four Lead Phosphates, $A_2PbBi_2(PO_4)_2(P_2O_7)$ (A = Rb, Cs) and $A_2PbP_2O_7$ (A = K, Rb), *Inorg. Chem.*, 2020, **59**, 2945–2951.

53 M. Cheng, W. Jin, Z. Yang and S. Pan, $Cs_3B_3O_3F_6$ with a Deep-Ultraviolet Cutoff Edge and a Suitable Birefringence as the Potential Zero-Order Waveplate Material, *Inorg. Chem.*, 2020, **59**, 13014–13018.